[3]Krogstad, P.-Å., Antonia, R. A., and Browne, L. W. B., "Comparison Between Rough- and Smooth-Wall Turbulent Boundary Layers," *Journal of Fluid Mechanics*, Vol. 245, 1992, pp. 599–617.

[4]Krogstad, P.-Å., and Antonia, R. A., "Surface Roughness Effects in Turbulent Boundary Layers," *Experiments in Fluids*, Vol. 27, No. 5, 1999, pp. 450–460.

[5]Townsend, A. A., *The Structure of Turbulent Shear Flow*, Cambridge Univ. Press, Cambridge, England, U.K., 1976, p. 139.

[6]Raupach, M. R., "Conditional Statistics of Reynolds Stress in Rough-Wall Turbulent Boundary Layers," *Journal of Fluid Mechanics*, Vol. 108, 1981, pp. 363–382.

[7]Andreopoulos, J., and Bradshaw, P., "Measurements of Turbulence Structure in the Boundary Layer on a Rough Surface," *Boundary-Layer Meteorology*, Vol. 20, No. 2, 1981, pp. 201–213.

[8]Miyake, Y., Tsujimoto, K., and Nakaji, M., "Direct Numerical Simulation of Rough-Wall Heat Transfer in a Turbulent Channel Flow," *International Journal of Heat and Fluid Flow*, Vol. 22, No. 3, 2001, pp. 237–244.

[9]Brown, A. R., Hobson, J. M., and Wood, N., "Large-Eddy Simulation of Neutral Turbulent Flow over Rough Sinusoidal Ridges," *Boundary-Layer Meteorology*, Vol. 98, No. 3, 2001, pp. 411–441.

[10]Goldstein, D., Handler, R., and Sirovich, L., "Modeling a No-Slip Flow Boundary with an External Force Field," *Journal of Computational Physics*, Vol. 105, No. 2, 1993, pp. 354–366.

[11]Saiki, E. M., and Biringen, S., "Numerical Simulation of a Cylinder in Uniform Flow: Application of a Virtual Boundary Method," *Journal of Computational Physics*, Vol. 123, No. 2, 1996, pp. 450–465.

[12]Goldstein, D. B., and Tuan, T.-C., "Secondary Flow Induced by Riblets," *Journal of Fluid Mechanics*, Vol. 363, 1998, pp. 115–151.

[13]Saiki, E. M., and Biringen, S., "Spatial Numerical Simulation of Boundary Layer Transition: Effects of a Spherical Particle," *Journal of Fluid Mechanics*, Vol. 345, 1997, pp. 133–164.

[14]Schlichting, H., *Boundary Layer Theory*, 7th ed., McGraw–Hill, New York, 1979, p. 616.

P. R. Bandyopadhyay
Associate Editor

Computational Simulation of the Air Wake over a Naval Transport Vessel

Martin J. Guillot*
University of New Orleans, New Orleans, Louisiana 70148

Introduction

NAVAL amphibious assault vessels transport personnel to and from operational areas. This is normally accomplished by operating some type of aircraft, for example, helicopters, from the deck of personnel transport ships. The ship topside structures produce an air wake over the deck in the operating region of the aircraft. The air wake is inherently unsteady due to vortex shedding from the topside structures. To understand the air wake and its possible effect on aircraft operations, it is necessary to quantify its main features. This Note presents time-averaged results of an unsteady computational simulation over a naval transport vessel. Experimental data are used to assess the accuracy of the computational results.

Previous researchers have computed the steady-state air wake over ships using various methods. For example, Tai and Carico[1] use a thin-layer Navier–Stokes method to compute the steady-state solution for the air wake over a landing helicopter deck (LHD) ship configuration. However, there is debate as to how to interpret results produced by a steady-state model when comparing to experimental data that was collected in a flowfield exhibiting global unsteadiness and then time averaged. Dolling[2] addresses this topic within the context of the supersonic compression ramp problem. Reynolds-averaged Navier–Stokes (RANS) computational fluid dynamics (CFD) models of supersonic compression ramps for large ramp angles where flow separation and reattachment occurs have historically shown poor agreement with experimental data for quantities such as mean surface pressure distribution and mean velocity profiles downstream of reattachment.[3–5] Dolling[2] asserts that the experimental flowfield exhibits global unsteadiness that is not captured by the steady-state solutions produced by RANS codes. He presents evidence indicating that better agreement with time-averaged experimental data might be obtained by a CFD computation that includes the global unsteadiness in the flowfield and then time averaged in the same manner as the experimental data.

In this effort, an unsteady computational simulation is performed on the topside airflow over a naval transport vessel. The results are time averaged, and the mean flow is compared to unsteady experimental data collected at the same frequency and time averaged in the same manner. Results are presented at selected points in the air wake over the aft deck of the vessel.

Experimental Study

In conjunction with the computational study, an experimental investigation into the air wake over a naval transport vessel was performed on a 1/94 subscale model in the 8 × 10 Foot Subsonic Wind Tunnel at the Naval Surface Warfare Center, Carderoc Division. The details of the experimental setup, procedures, data reduction, and results are reported by Guillot and Walker.[6] Data were collected at 500 Hz for 4.096 s.

The experimental accuracy is determined postexperiment by examining the mean square error in each probe's calibration curve, combined with an analysis of data taken at a freestream reference point during each run. The freestream reference point analysis is meant to account for individual probe response, which can change due to dirt accumulation on the sensor, plus any residual effects from ambient temperature variations. The expected confidence in the experimental data is ±5%.

Computational Simulatons

The ship geometry and coordinate system used in the computations are shown in Fig. 1. There are two helicopter landing pads on the aft deck, located at $x = 153.5$ and 188.0 m. The results presented here focus on the aft landing pad, $x = 188.0$ m and on the ship centerline.

The computational analysis was performed using FAST3D.[7] FAST3D, developed at the U.S. Naval Research Laboratory, is capable of solving the three-dimensional unsteady compressible Euler equations on parallel architectures using Cartesian meshes. It employs the flux-corrected transport method with virtual cell embedding to resolve internal boundaries in the flowfield.

Wind angles of 0 and 30 deg with respect to the ship centerline were studied with a nominal incoming velocity of 30 kn (15.34 m/s). To complete the description of the computational model, appropriate boundary conditions were prescribed. The locations of lateral boundaries were chosen to match the dimensions of the wind tunnel. The forward boundary was chosen to be one ship length ahead

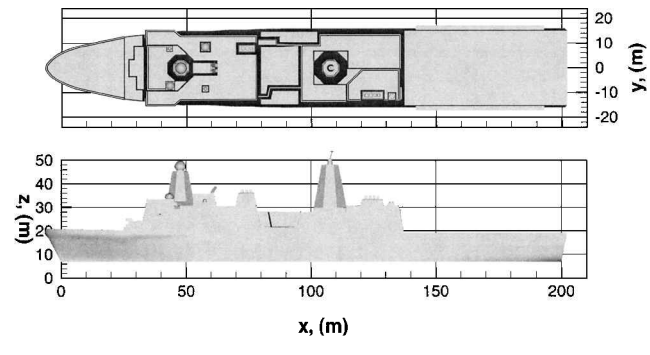

Fig. 1 Ship geometry and coordinate system.

Received 1 November 2001; revision received 15 December 2001; accepted for publication 9 June 2002. Copyright © 2002 by the American Institute of Aeronautics and Astronautics, Inc. All rights reserved. Copies of this paper may be made for personal or internal use, on condition that the copier pay the $10.00 per-copy fee to the Copyright Clearance Center, Inc., 222 Rosewood Drive, Danvers, MA 01923; include the code 0001-1452/02 $10.00 in correspondence with the CCC.

*Assistant Professor, Department of Mechanical Engineering, 2000 Lakeshore Drive.

of the forwardmost point of the ship so that freestream incoming boundary conditions could be imposed. The aft boundary was chosen to be far enough downstream so that it could be assumed that gradients in the x direction were zero. Zero normal flow is imposed at the ship surface and all lateral boundaries. The freestream velocity is specified at the inlet. Downstream, an extrapolation boundary condition is imposed. The compressible Euler equations also require specification of ambient pressure and density. The pressure and density were specified to be standard atmospheric conditions at sea level. For the 30-deg case, the ship is rotated counterclockwise about the ship centerline at $x = 153.5$ m.

For the computational simulations, the 0-deg grid contained $416 \times 96 \times 128$ volumes, and the 30-deg case contained $416 \times 96 \times 256$ volumes. A detailed error analysis of the flux-corrected transport method is provided by Boris and Book.[8] To establish numerical solution convergence, grid and time-step independence studies were performed for the 0-deg case. The 0-deg case was run with a time step of one-half initial runs, and the number of volumes in the x direction was doubled. The results were compared to the initial runs, and the solutions were observed to change less than 1% at the considered locations. From these results, it was concluded that the computed solution was grid and time-step independent.

Data Reduction

The results of the computational and experimental analysis consist of velocity time histories (u, v, w) at 279 data locations above the aft deck. Experimentally and computationally, data were collected at 500 Hz, that is, every 0.002 s, for a total of 4.094 s, giving a total of 2048 data samples at each data location. The CFD simulations were run for 4.594 s, and the first 0.5 s of computational data were discarded to eliminate the effect of the transient startup. From the time histories, the average velocity at each data location is computed by summing the velocity samples and dividing by the total number of samples. The time-averaged velocities

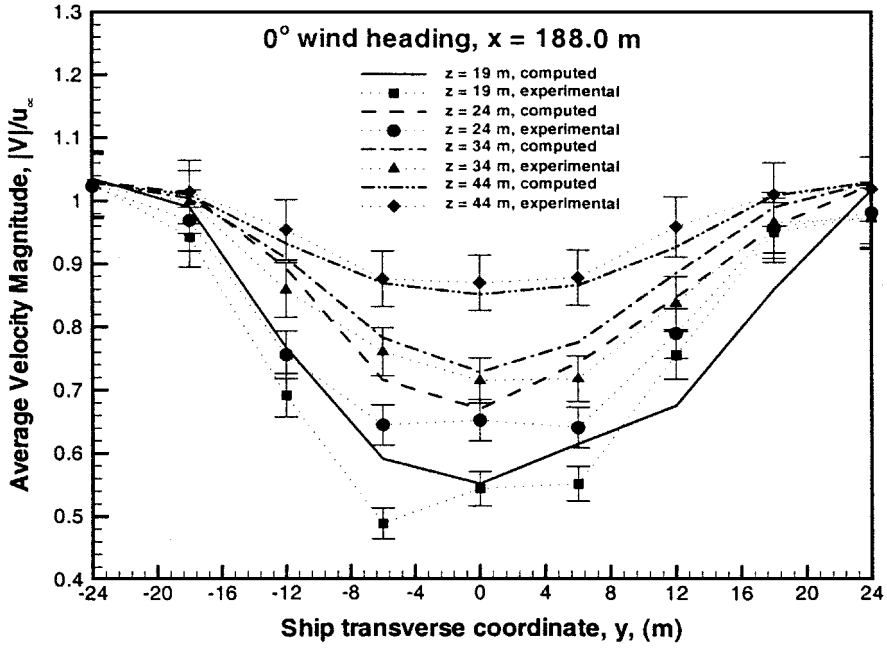

Fig. 2 Average velocity magnitude over aft deck at $x = 188.0$ m, 0-deg wind.

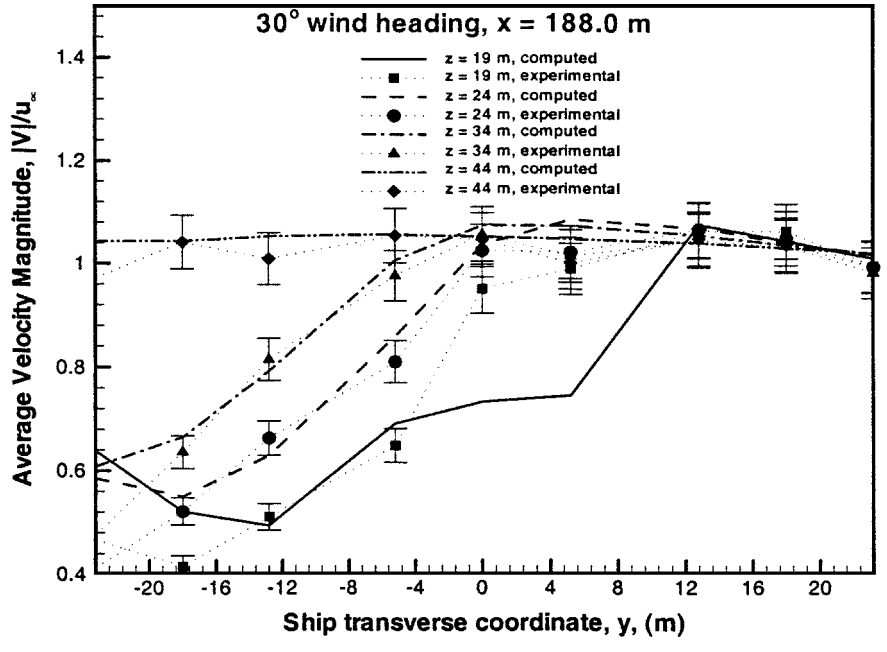

Fig. 3 Average velocity magnitude over aft deck at $x = 188.0$ m, 30-deg wind.

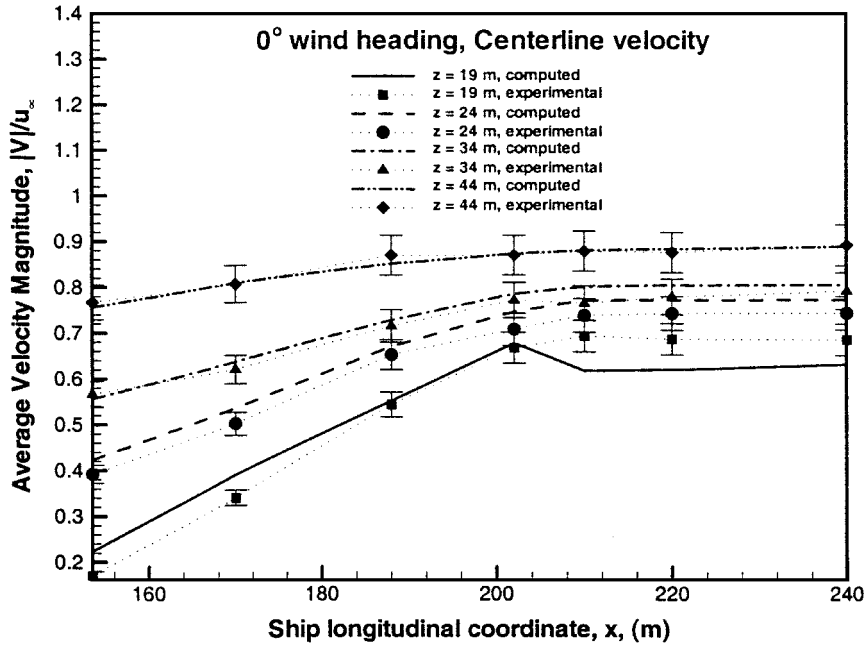

Fig. 4 Average centerline velocity magnitude over aft deck, 0-deg wind.

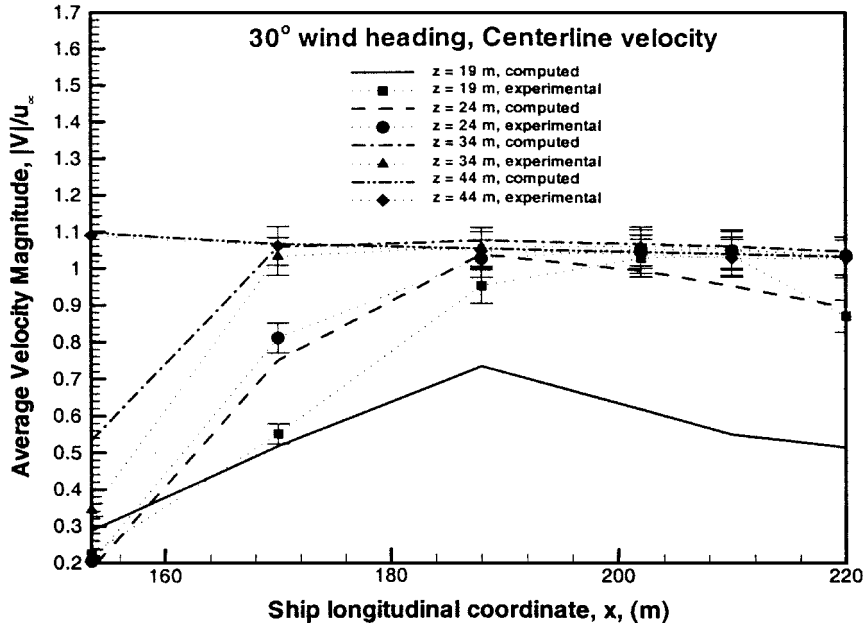

Fig. 5 Average centerline velocity magnitude over aft deck, 30-deg wind.

are nondimensionalized by the incoming freestream velocity for presentation.

Results

Figures 2 and 3 show mean velocities across the ship deck from port to starboard for the 0- and 30-deg cases, respectively. Four values of z are shown in Figs. 2 and 3. Figures 2 and 3 clearly show the velocity deficit behind the topside structures. In each of the cases, the velocities approach approximately $1.05u_\infty$ toward the edges of the ship. This is expected because the presence of the ship in the wind tunnel causes a slight acceleration of the freestream above the ship. The 0-deg case displays a more symmetrical profile with respect to the centerline, whereas the 30-deg case shows the velocity deficit shifted to the port side.

Figures 4 and 5 show the mean centerline velocity profiles at several elevations above the deck for the 0- and 30-deg cases, respectively. Figures 4 and 5 generally indicate a recovery of the velocity toward freestream values as the flow proceeds over the aft portion of the deck to the rear of the ship.

Conclusions

It is concluded that the CFD computations of the ship air wake provide a reasonably accurate description of the time-averaged flow for the cases considered. Generally, the trend is that there is better agreement between computations and experimental data for the higher elevations, away from the surface of the deck. For both wind angles, many of the computed results lie within the experimental error of ±5%. For the 0-deg case, all computational results agree to within 20% of the experimental data. The largest disagreement occurs for the 30-deg case at $z = 19$ m.

References

[1]Tai, T. C., and Carico, D., "Simulation of DD-963 Ship Air Wake by Navier–Stokes Method," AIAA Paper 93-3002, July 1993.

[2]Dolling, D., "Problems in the Validation of CFD Codes Through Comparison with Experiment," *AGARD Symposium on Theoretical and Experimental Methods in Hypersonic Flows*, CP-514, AGARD, 1993, pp. 19.1–19.15.

[3]Viegas, J. R., and Horstman, C. C., "Comparison of Multi-Equation Turbulence Models for Several Shock/Boundary-Layer Interaction Flows," *AIAA Journal*, Vol. 17, No. 8, 1970, pp. 811–820.

[4]Horstman, C. C., "Prediction of Hypersonic Shock Wave/Turbulent Boundary-Layer Interaction Flows," AIAA Paper 87-1367, June 1987.

[5]Wilcox, D. D., "Supersonic Compression Corner Applications of a Multi-Scale Model for Turbulent Flows," *AIAA Journal*, Vol 78, No. 7, 1990, pp. 1194–1198.

[6]Guillot, M. J., and Walker, M. A., "Unsteady Analysis of the Air Wake over the LPD-17," AIAA Paper 2000-4125, Aug. 2000.

[7]Boris, J. P., Landsberg, A. M., Oran, E. S., and Gardner, J. H., "LCPFCT—A Flux-Corrected Transport Algorithm for Solving Generalized Continuity Equations," Lab. for Computational Physics, U.S. Naval Research Lab., NRL Memorandum Rept. 93-7192, 1993; also URL: http://www.lcp.nrl.navy.mil/lcpfct.

[8]Boris, J. P., and Book, D. L., "Solution of Continuity Equations by the Method of Flux-Corrected Transport," *Methods in Computational Physics*, edited by B. Alder, S. Fernbach, and M. Rotenberg, Vol. 16, Academic Press, New York 1976, pp. 85–129.

P. R. Bandyopadhyay
Associate Editor

Layer-by-Layer Analysis of a Simply Supported Thick Flexible Sandwich Beam

Hemendra Arya,* R. P. Shimpi,† and N. K. Naik†
Indian Institute of Technology Bombay, Mumbai 400 076, India

Introduction

MODERN sandwich structures consist of stiff faces, often unsymmetrical, and plastic foam as core, which is flexible in nature. To analyze such a structure, a theory is needed that can account for the transverse flexibility of the core and shear deformation. Traditionally, sandwich structures are analyzed using Timoshenko theory, in which the shear stress distribution is assumed to be constant across the thickness and the core is assumed to be rigid in transverse direction (see Ref. 1). A refinement to such a theory is a higher-order displacement field, where shear stress distribution is not assumed constant. Such refinements can account for shear deformation very easily, but transverse flexibility is not accounted for. A further refinement is to enhance the core analysis where transverse flexibility can be accounted for. Frostig et al.[2] developed a sandwich beam theory that accounts for core flexibility. This theory is extended by Swanson[3] for multiple supports and overhang. Recently, Pai[4] and Perel and Palazotto[5] developed finite element for flexible core sandwich structures. A good review on sandwich structures is given in Ref. 6.

In the present work, a simply supported sandwich beam of isotropic layers is considered. The two thin stiff faces are connected to a flexible core. The thin faces are analyzed using classical beam theory, where the assumptions of the plane section remaining plane and constant thickness are applicable. The thick core is analyzed using a more involved solution, that is, two-dimensional elasticity theory under plane stress conditions.[7] This two-dimensional solution, being general in nature, will account for transverse flexibility of the core, as well as shear deformation. This technique reduces the complexity of the solution as compared to if all of the layers are analyzed a using two-dimensional solution for such a problem.

In the present formulation, in-plane and transverse displacement boundary conditions are satisfied at the interface. The shear stress at the interface is modeled as moment and an in-plane force in the face.

For comparison, results of a solution is also obtained for the sandwich beam when all of the three layers are analyzed using two-dimensional elasticity under plane stress conditions. Present results are also compared with a conventional higher-order theory and a layer-by-layer theory referred to as trigonometric shear deformation theory–equivalent single layer (TSDT-ESL) and TSDT–zig zag (TSDT-ZZ). The displacement field and governing equations for these refined theories are given in Ref. 8.

Formulation of the Problem

A schematic diagram of the sandwich beam is shown in Fig. 1a. Let Young's modulii of the top face be E_t, the core be E_c, the bottom face be E_b, and Poisson's ratio of the core be ν_c. The thickness of the top face is t_t, that of the core is h_c, and that of the bottom face is t_b. The beam width is b.

The top and bottom faces are taken as a beam connected to an elastic core. The various stresses acting on the skins and core are shown in Fig. 1b. The shear stress at the interface is modeled as an in-plane load and a moment in the skin for the analysis as shown in Fig. 1c.

Let the lateral loading at the top of the top face be q and

$$q = \sum_{m=1}^{\infty} E_m \sin\alpha x, \qquad E_m = \frac{2}{l}\int_0^l q \sin\alpha x \, \mathrm{d}x \tag{1}$$

The stresses acting on the core are represented in series form, at the top of the core

$$\sigma_y = \sum_{m=1}^{\infty} -B_m \sin\alpha x, \qquad \tau_{xy} = \sum_{m=1}^{\infty} C_m \cos\alpha x \tag{2}$$

and at the bottom of the core

$$\sigma_y = \sum_{m=1}^{\infty} -A_m \sin\alpha x, \qquad \tau_{xy} = \sum_{m=1}^{\infty} D_m \cos\alpha x \tag{3}$$

where $\alpha = m\pi/l$ and l is the length of the beam and E_m is constant and depends on loading on the top face. A_m, B_m, C_m, and D_m are unknowns.

Solution for the Top Face

Figure 1c shows the loads acting on the top face. The lateral deflection v_t of the top face is assumed in terms of unknown constant S_m as

$$v_t = \sum_{m=1}^{\infty} S_m \sin\alpha x \tag{4}$$

From Fig. 1c, note that lateral loading and distributed moment in the top face is

$$q_y = \sum_{m=1}^{\infty} \sin\alpha x (E_m - bB_m), \qquad T_x = \frac{bt_t}{2}\sum_{m=1}^{\infty} C_m \cos\alpha x \tag{5}$$

Received 15 February 2002; revision received 1 June 2002; accepted for publication 8 June 2002. Copyright © 2002 by the American Institute of Aeronautics and Astronautics, Inc. All rights reserved. Copies of this paper may be made for personal or internal use, on condition that the copier pay the $10.00 per-copy fee to the Copyright Clearance Center, Inc., 222 Rosewood Drive, Danvers, MA 01923; include the code 0001-1452/02 $10.00 in correspondence with the CCC.

*Research Associate, Aerospace Engineering Department, Powai; currently Research Scientist, Center for Aerospace Systems Design and Engineering, Indian Institute of Technology Bombay, Mumbai 400 076, India; arya@aero.iitb.ac.in.

†Professor, Aerospace Engineering Department, Powai.